Nanowire heterostructures

DOI: 10.1002/smll.200700892

High-Quality InAs/InSb Nanowire Heterostructures Grown by Metal–Organic Vapor-Phase Epitaxy**

Philippe Caroff, Jakob B. Wagner, Kimberly A. Dick, Henrik A. Nilsson, Mattias Jeppsson, Knut Deppert, Lars Samuelson, L. Reine Wallenberg, and Lars-Erik Wernersson*

Recently, semiconducting nanowires have attracted much interest due to their advantageous physical properties and a wide range of potential applications in electronics,[1] optoelectronics,[2] and biosensors.[3,4] High-quality compound nanowire heterostructures have been grown using various techniques, including chemical-beam epitaxy (CBE)[5] and metal–organic vapor-phase epitaxy (MOVPE),[6] with both methods producing sharp interfaces. To date, most studies have concentrated on ''classic'' III–V semiconductors, such as InAs, InP, GaAs, GaP, and nitride nanowires. Antimony-containing nanowires would extend the range of usable materials in these heterostructures and devices. InSb is the III–V semiconductor with the narrowest bandgap (0.17 eV) and the largest bulk electron mobility ($\approx 7.7 \times 10^4\,cm^2\,V^{-1}\,s^{-1}$);[7] it also has a high thermoelectric figure of merit (0.6).[8] This material is therefore extremely interesting for applications in high-speed and low-power electronics, infrared optoelectronics, quantum-transport studies, and thermoelectric power generation. Despite all of these promising advantages, very few studies on InSb nanowires have been reported.[8–10] There have so far been no reports on InSb-containing nanowire heterostructures. Moreover, due to the large lattice mismatch between InAs and InSb (7%), no combination of these materials has been reported using planar growth. In this Communication, we demonstrate for the first time growth of high-quality InAs/InSb heterostructure nanowires.

[*] Dr. P. Caroff, Dr. J. B. Wagner, Dr. K. A. Dick, H. A. Nilsson, M. Jeppsson, Prof. K. Deppert, Prof. L. Samuelson, Prof. L.-E. Wernersson
Solid State Physics/The Nanometer Structure Consortium
Lund University
Box 118 SE-22100 Lund (Sweden)
Fax: (+46) 462-223-637
E-mail: philippe.caroff@ftf.lth.se
Dr. J. B. Wagner, Prof. L. R. Wallenberg
Polymer and Materials Chemistry/nCHREM
Box 124 SE-22100 Lund (Sweden)

[**] The authors thank Brent A. Wacaser and Werner Seifert for valuable discussions. This work was carried out within the Nanometer Structure Consortium in Lund and was supported by the Swedish Foundation for Strategic Research (SSF), the Swedish Research Council (VR), the European Community (EU contract no. 015783 NODE), and the Knut and Alice Wallenberg Foundation.

Supporting Information is available on the WWW under http://www.small-journal.com or from the author.

The InAs/InSb nanowire heterostructures were grown on InAs(111)B substrates decorated with 40-nm-diameter gold aerosol particles.[11] All samples were grown in a conventional horizontal MOVPE reactor. The InAs segment was grown using trimethylindium (TMIn) and arsine; the arsine was then switched off and trimethylantimony (TMSb) was switched on to grow the InSb segment. The growth was terminated by shutting off the TMIn and TMSb sources simultaneously, and cooling down was performed under hydrogen flow only. Both segments were grown at 460 °C for a few minutes each. The samples were characterized using scanning electron microscopy (SEM) and field-emission gun transmission electron microscopy (FEG-TEM), the latter equipped with an X-ray energy-dispersive spectroscopy module (X-EDS). A brief electric characterization was also performed. A more detailed description of the procedures can be found in the Experimental Section.

The growth parameters were thoroughly studied, including the effects of aerosol particle size, temperature, growth duration, V/III ratio, and molar fraction. Reproducibility was achieved using proper cleaning of the reactor prior to each growth run. A detailed analysis of the growth parameters is not the focus of this Communication and will be presented elsewhere. Only the most striking features will be considered here. Characteristic examples of the nanowires are shown in Figure 1a and 1b, obtained using SEM and TEM, respectively. All nanowires grow in the [111]B direction. We observe that the nanowires have a two-segment structure with a narrow base diameter and a wide upper-segment diameter. These two segments are determined to be InAs and InSb, as will be shown below, and will therefore be referred to as such here. The InAs segments are 600 nm long on average, with a top diameter of 50 ± 3 nm, while the InSb segments are 350 nm long with a diameter of 70 ± 3 nm. The InAs segments are found to be tapered, whereas the InSb segments are nontapered. It should be noted that it was not possible to grow straight nanowires in the opposite direction (InSb/InAs) under the conditions used in this study. This can be explained by the relative interface energies between the particle and the two semiconductor materials, as explained by a recent model.[12] Further work is ongoing to solve this challenge.

Figure 1a shows a bright-field TEM image of the nanowire heterostructure. Contrast from strain fields is clearly visible below the wider segment and originates from the junction between the InAs and InSb. This strain field is due to the very large lattice mismatch of 7% at the interface between the two materials, similar to observations for InAs/InP heterostructure interfaces.[13] At the top of the nanowires, we observe a fully facetted particle, visible on both Figure 1a and 1b.

To gain more information on the structure of the nanowire, high-resolution TEM investigations of several nanowires (>10) were conducted and the results for the lower and upper parts of the nanowire are shown in Figure 2a and b, respectively. The lattice fringe image and its associated fast Fourier transform (FFT) in Figure 2a confirm the high-quality single-crystal InAs base, which has a wurtzite structure. The nanowire changes from wurtzite to zinc blende InAs at an atomically sharp interface (marked in Figure 2a with white broken lines). The origin of this change of structure will be

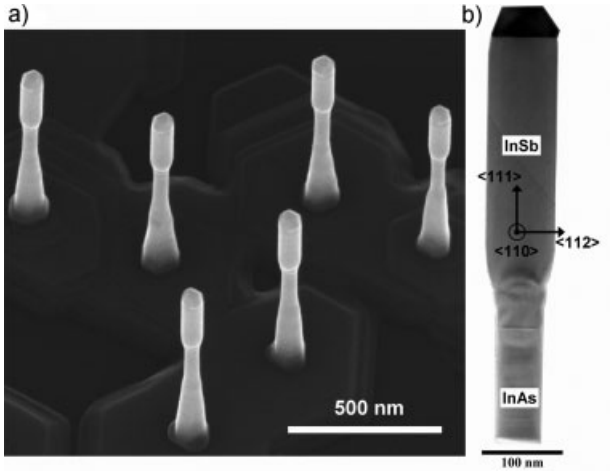

Figure 1. a) SEM image of the InAs/InSb wires grown on a InAs(111)B substrate, tilted by 30° and b) bright-field TEM image along the [$\bar{1}$10]direction (InSb segment) of a nanowire from the same sample after detachment from the substrate.

briefly discussed below. The zinc blende InAs segment is on average 40 nm long. Both InAs crystal structures show a very low density of stacking faults; they are estimated to be around 1% in the InAs wurtzite and InAs zinc blende segments for all investigated nanowires. Furthermore, Figure 2a shows the interface where the composition changes from InAs to InSb. The corresponding FFT demonstrates that both this InAs segment and the InSb segment have zinc blende crystal structures. The interface is atomically sharp as the lattice-fringe separation parallel to the interface changes abruptly at the interface. The relaxation perpendicular to the interface is found to extend approximately 10 nm on each side of the interface, similar to the relaxation observed in other nanowire heterostructures.[14] These two sharp interfaces are observed on all measured nanowires.

Figure 2b shows the upper part of the nanowire where a sharp interface between InSb and the particle is clearly visible. No stacking faults or twinning could be observed in the InSb segment of our nanowires. The FFT confirms that the particle on top of the InSb segment is single crystalline, with a cubic crystal structure matching an $AuIn_2$ structure. Furthermore, the crystal orientation of the particle is always found to be twinned compared to the InSb segment, as exemplified in the FFTs in Figure 2b. The dim extra spots present in the FFT in the ⟨111⟩ directions are most probably due to ordering of antimony atoms in the structure, as discussed below. The facets of the particle that correspond to the {111} and {100} facets are recognizable in the SEM images. From these facets and from the independent observation that the hexagonal nanowire macrofacets are found to be parallel to {110} cleavage planes of the sample, the orientation of the InSb segment side facets can be determined from SEM images. The InSb segment side macrofacets are found to have {110} orientations. Moreover, no microfaceting of the nanowire side walls is observed as they appear to be straight in TEM images viewed along both the ⟨110⟩ and ⟨112⟩ zone axis. Higher-resolution images of all interfaces and details of the particle facets are provided as Supporting Information.

The structural perfection of the nanowires has been demonstrated by the TEM analysis shown on the electron micrographs in Figure 2. X-EDS analysis was used to investigate the chemical composition of the nanowire segments and interfaces using both line scans and point analysis. The statistical point-analysis study was performed on 10 nanowires in three regions of interest: the InAs segment, the InSb segment, and the seed particle. Figure 3a shows the scanning TEM (STEM) and corresponding X-EDS line scan of the InAs/InSb interface. On the X-EDS line scan, it is observed that the nanowire starts as InAs and then changes to InSb. Since the lattice parameter is observed (by FFT analysis) to change abruptly at this interface, the gradient observed for the antimony signal is believed to result from the limited spatial resolution of the X-EDS spectra due to scattering effects in combination with a small overgrowth of InSb on the InAs part closest to the InSb segment. The thickness of this overgrowth varies slightly from nanowire to nanowire.

The apparent change in indium content between the two segments is related to an increased signal from the thicker InSb segment. Point analysis of the InAs segment gives a 49.5 to 50.5 ratio (±0.6) between indium and arsenic, with no trace of any other material. The margin of error represents the statistical deviation in the EDS measurements. In the InSb segment, a 49.3 ± 1.3 to 48.5 ± 1.1 ratio between indium and antimony is measured with a small amount, $2.2 \pm 0.3\%$, of arsenic detected in the segment. This may indicate some residual background arsenic in the InSb segment. The upper part of the nanowire has been studied in the same way and is shown in Figure 3b, where the InSb-to-particle transition and the corresponding X-EDS line scans are presented. The composition of the remaining particle is found to be an alloy of indium and gold. The measured composition is $28.5 \pm 0.8\%$ of gold and $68.0 \pm 0.8\%$ of indium, with a small amount of antimony $3.5 \pm 0.6\%$. Gold and indium are known to alloy in a CaF_2 crystal structure.[15] The lattice-fringe separation and composition in the present study each coincides with a $AuIn_2$ single crystal. The small amount of antimony is thought to substitute some of the gold atoms. Moreover, we observe an indium-containing shell with no gold or antimony surrounding the particle, as shown in both Figures 2b and 3b.

Electrical characterization of the InSb nanowire segment was carried out after transfer to a silicon substrate. The sample growth conditions only differ from those previously analyzed by the use of reduced molar fractions and longer growth time, to ensure a more practical length of the InSb segment (1 μm). A typical contacted InSb segment is illustrated in Figure 4a. More details of the processing can be found in the experimental section and in the work of Thelander et al.[16] The *I–V* characteristics measured at 300 K and 4.2 K and zero-backgate voltage are presented in Figure 4b. A linear behavior is clearly observed at both temperatures, suggesting good ohmic contacts. Resistances of 15 kΩ and 7 kΩ are measured at 300 K and 4.2 K, respectively. The source–drain current plotted as a function of the backgate voltage is reported in Figure 4c. The InSb nanowire segment shows n-type behavior, as applying a positive (negative) backgate voltage increases (decreases) the conductivity. These results constitute a preliminary study. A detailed analysis of the

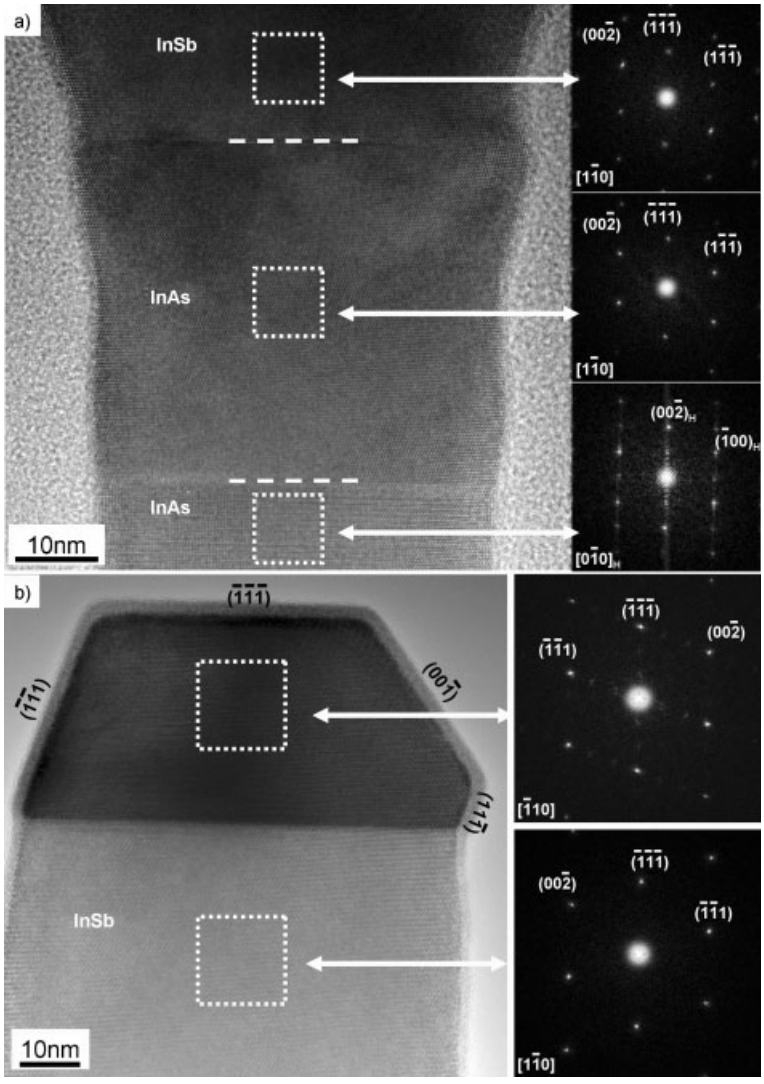

Figure 2. a) High-resolution TEM lattice-fringe image along the $[1\bar{1}0]$ direction of the InAs/InAs and InAs/InSb interfaces and corresponding FFT of the three regions of interest. The two white broken lines are a guide to the eye for the interface between InAs wurtzite/InAs zinc blende and InAs zinc blende/InSb zinc blende.
b) High-resolution TEM lattice-fringe image along the $[1\bar{1}0]$ direction of the InSb/seed-particle interface and FFTs of the two regions of interest. Images of higher magnification are in the Supporting Information.

electrical characteristics of the full InAs/InSb heterostructure nanowires will be presented elsewhere.

Discussion and interpretation of the presented results follow below. First, the large change of diameter observed at the InAs/InSb interface is very unusual in heterostructure nanowires. For example, a small diameter variation (3%, corresponding to the lattice mismatch) is observed when switching from InAs to InP,[14] whereas here a diameter increase of 40% occurs. Only one other group has shown a comparable increase of the diameter in a III–V system when growing GaAs/GaSb nanowires.[17] In their system, the diameter increase was explained by strain-relaxation effects. In our system, the particle composition analysis led us to postulate another mechanism to explain this remarkable feature. In contrast to previous results on InAs nanowires grown under similar conditions as this study, where the indium content in the particle was found in the range of 25–32%,[18,19] the detailed X-EDS analysis showed that in this case the particle on top of the InSb segment contains 67% indium. Assuming a similar indium content during and after InSb growth and an indium content of 30% in the particle during InAs growth, a simple calculation can be performed using the atomic volumes of gold and indium. We determine that the difference in indium concentration in the particle from 30 to 67 atomic percent would lead to an increase of the particle diameter of 35%. Furthermore, this is consistent with the experimentally determined increase in AuIn alloy particle diameter with indium content reported by Dick et al.[20] Although this study is a post-growth study and the composition of the particle might be different under growth, we suggest that the change of the particle volume due to uptake of indium is the main reason for the nanowire diameter increase when growing InSb.

The fact that such a high indium content is found in the particle after InSb nanowire growth, and not in the InAs nanowire system, may be explained by considering the appropriate Au–In–As and Au–In–Sb ternary systems.[21,22] The Au–In–Sb system differs from the Au–In–As system in that there is a stable intermediate compound $AuSb_2$; no such intermediate AuAs compounds exist. The stability of this compound means that the triangulation of the ternary systems is fundamentally different. AuIn compounds with low indium content (less than 50 atomic percent) form pseudo binary systems with InAs; the same is not true for InSb. This means that InAs nanowires can grow from a supersaturated AuIn γ-phase particle (about 30 atomic percent indium) but this will not occur for InSb. The $AuIn_2$–InSb system is known to be a pseudo binary eutectic system with up to 12% InSb soluble in $AuIn_2$. This suggests that InSb could be precipitated from a supersaturated liquid particle (leaving $AuIn_2$) or from a supersaturated solid $AuIn_2$ particle (which can dissolve about 2 atomic percent antimony). Since our growth temperature is below, but close to, the eutectic temperature of 472 °C, it is not clear which is more likely. In fact, both solid and liquid particles may be involved even at the same growth temperature, as has been reported for germanium nanowires.[23] In that case, wires grew more slowly from solid gold alloy particles, perhaps due to the very low diffusivity of Ge in solid gold. By contrast, indium has a very high diffusivity in solid gold and would not be expected to be growth-rate limiting. Therefore, wires grown from solid and liquid particles cannot be distinguished by their growth rate. It should be emphasized that the in situ composition of the particle will not match the composition determined by post-growth analysis; the particle will instead be supersaturated with InSb. It should also be noted that the region of the ternary-phase diagram in

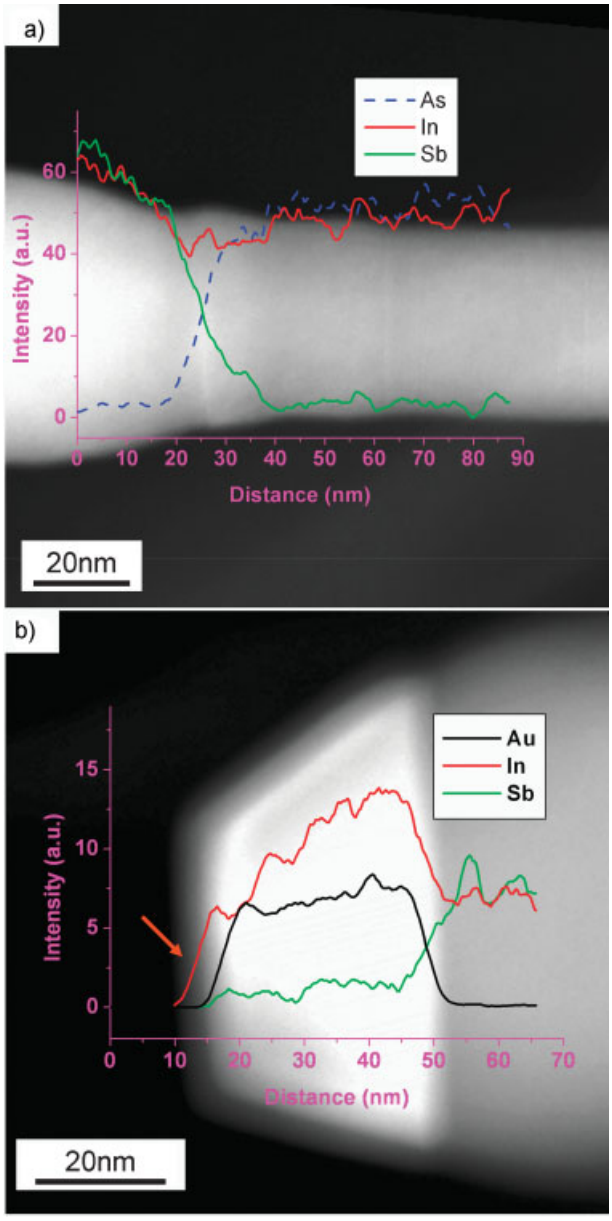

Figure 3. a) STEM image of the nanowire in the [1$\bar{1}$0] direction in the region of the InAs/InSb interface, with corresponding normalized X-EDS line scan superimposed (blue = As, red = In, green = Sb). b) STEM image in the ⟨110⟩ direction of the InSb/seed-particle interface of the nanowire, with the corresponding normalized X-EDS line scan superimposed (black = Au, red = In, green = Sb). The red arrow on the graph shows the presence of an In-rich shell around the particle.

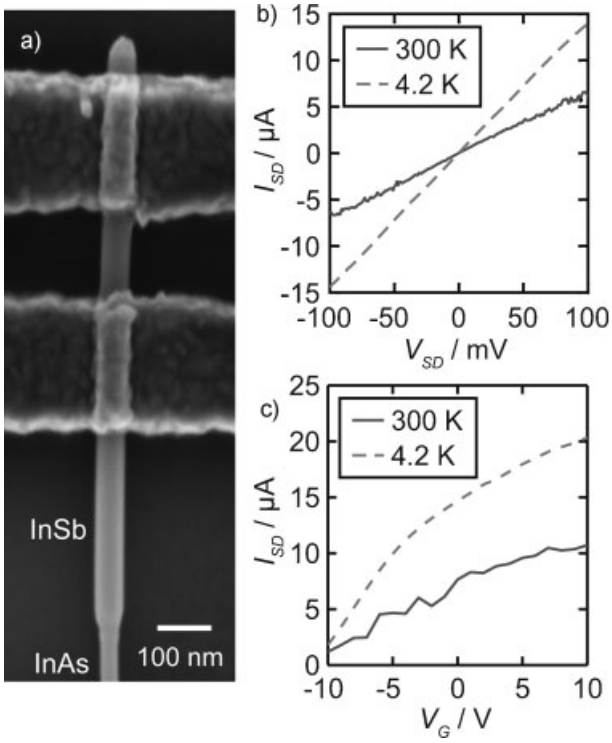

Figure 4. a) SEM image of typical electrically contacted InSb nanowire segment. The distance between the two contacts is 200 nm. b) *I–V* curves for an InSb nanowire segment 70 nm in diameter, recorded with a backgate voltage set to zero, at 300 K and 4.2 K. c) Source–drain current trough the InSb nanowire segment plotted as a function of the backgate voltage for $V_{s-d} = 100$ mV at 300 K and 4.2 K.

which growth occurs will depend on the relative precursor flows, as well as temperature and pressure. The low V/III ratio used for InSb growth may favor a particle composition with higher indium content.

The crystal perfection of the InSb segment may be explained by lattice matching at the Au(Sb)In_2/InSb interface (only in the case of a vapor–solid–solid growth mechanism) but the nature of InSb itself also has to be considered. The lower ionicity of InSb (0.303)[24] compared with most other III–V compounds decreases the probability of creating stacking faults and favors a pure zinc blende nanowire. Another remarkable feature concerns the abrupt change in crystal structure for InAs during growth. The 40-nm-long InAs zinc blende segment is always present below the InAs/InSb interface and is thus assumed to correspond to the gas-switching sequence from arsine to TMSb. The mechanisms behind the change of crystal structure in the InAs segment are not fully understood yet but are thought to be affected by a change of the effective V/III ratio.[25] The effective V/III ratio is reduced upon switching between arsenic and antimony precursors. Furthermore, antimony is known to act as a surfactant in many systems and could affect the migration length on the surface or at the growing interface, leading to an additional change of the effective V/III ratio.[26,27] A more detailed analysis of the change of crystal structure in InAs is still under investigation.

In summary, we have demonstrated epitaxial InSb nanowire grown by MOVPE without stacking faults and have shown the possibility of combining it with InAs to form a heterostructure with very sharp interfaces. The InSb segment has a diameter increased by 40% compared to the InAs, which is explained by a change of the seed-particle composition and size. The remaining particle on top of the InSb segment is found to be single-crystalline Au(Sb)In_2, lattice matched to the InAs/InSb crystal. The transitions of InAs from wurtzite to zinc blende and then from InAs zinc blende to InSb zinc blende single-crystal structure show very high structural

quality and are promising for future InSb-containing nanowire heterostructure devices. Moreover, the preliminary electrical characterization proves that InSb forms ohmic contacts with electrodes similarly to InAs, which opens the way to transport measurements for this very narrow bandgap material.

Experimental Section

Nanowire growth procedure: The sample was grown at a reactor pressure of 100 mbar in a conventional horizontal MOVPE reactor using TMIn, AsH_3, and TMSb as source materials. The temperature was ramped to the nanowire growth temperature of 460 °C under AsH_3 flow. Growth was initiated by switching the TMIn flow to the reactor to grow InAs for 2 min; the AsH_3 was then switched off and TMSb was simultaneously switched on to initiate growth of the InSb segment. Growth of InSb was performed for 5 min. The TMIn molar fraction was kept at 1.4×10^{-5} for both InAs and InSb growth sequences. The growth was terminated by shutting off the TMIn and TMSb sources simultaneously and cooling was performed under hydrogen flow only. The molar fractions of AsH_3 and TMSb were 1.2×10^{-3} and 1.0×10^{-4}, respectively, corresponding to a nominal V/III ratio of 84 for the InAs segment and 7.3 for the InSb segment.

Electron microscopy: The sample was characterized using an FEI SEM at a working distance of 5.2 mm and an accelerating voltage of 20 kV. TEM characterization was performed on a JEOL 3000F field-emission gun TEM operating at 300 kV. As-grown nanowires were transferred to the TEM grid by gently touching the substrate with a standard lacey carbon TEM grid. Chemical composition of the nanowires was evaluated using both line scan and point analysis using an X-EDS module.

Electrical characterization: The nanowires were transferred to a degenerately doped Si substrate covered with a 100-nm layer of SiO_2 thermal oxide. Metal contacts were realized by electron-beam lithography, Ni/Au evaporation, and lift-off. Prior to metal evaporation, the wires were etched in an $(NH_4)_2S_x$ solution to remove the native oxide. The two metal electrodes were separated by 200 nm on average.

Keywords:
heterostructures · indium antimonide · MOCVD · nanowires · TEM

[1] C. Thelander, P. Agarwal, S. Brongersma, J. Eymery, L. F. Feiner, A. Forchel, M. Scheffler, W. Riess, B. J. Ohlsson, U. Gösele, L. Samuelson, *Mater. Today* **2006**, *7*, 28–35.
[2] P. J. Pauzauskie, P. Yang, *Mater. Today* **2006**, *10*, 36–45.
[3] K. Yang, H. Wang, K. Zou, X. Zhang, *Nanotechnology* **2006**, *17*, S276–S279.
[4] F. Patolsky, B. P. Timko, G. Zheng, C. M. Lieber, *MRS Bull.* **2007**, *32*, 142–149.
[5] M. T. Björk, C. Thelander, A. E. Hansen, L. E. Jensen, M. W. Larsson, L. R. Wallenberg, L. Samuelson, *Nano Lett.* **2004**, *4*, 1621–1625.
[6] M. T. Borgström, M. A. Verheijen, G. Immink, T. de Smet, E. P. A. M. Bakkers, *Nanotechnology* **2006**, *17*, 4010–4013.
[7] J. Riikonen, T. Tuomi, A. Lankinen, J. Sormunen, A. Säynätjoki, L. Knuuttila, H. Lipsanen, P. J. McNally, L. O'Reilly, A. Danilewsky, H. Sipilä, S. Vaijärvi, D. Lumb, A. Owens, *J. Mater. Sci.: Mater. Electron.* **2005**, *16*, 449–453.
[8] J. H. Seol, A. L. Moore, S. K. Saha, F. Zhou, L. Shi, Q. L. Ye, R. Scheffler, N. Mingo, T. Yamada, *J. Appl. Phys.* **2007**, *101*, 023706.
[9] H. D. Park, S. M. Prokes, M. E. Twigg, Y. Ding, Z. L. Wang, *J. Cryst. Growth* **2007**, *304*, 399–401.
[10] Y. Yang, L. Li, X. Huang, G. Li, L. Zhang, *J. Mater. Sci.* **2007**, *42*, 2753–2757.
[11] M. H. Magnusson, K. Deppert, J.-O. Malm, J.-O. Bovin, L. Samuelson, *Nanostruct. Mat.* **1999**, *12*, 45–48.
[12] K. A. Dick, S. Kodambaka, M. C. Reuter, K. Deppert, L. Samuelson, W. Seifert, L. R. Wallenberg, F. M. Ross, *Nano Lett.* **2007**, *7*, 1817–1822.
[13] M. T. Björk, B. J. Ohlsson, T. Sass, A. I. Persson, C. Thelander, M. H. Magnusson, K. Deppert, L. R. Wallenberg, L. Samuelson, *Appl. Phys. Lett.* **2002**, *80*, 1058–1060.
[14] M. W. Larsson, J. B. Wagner, M. Wallin, P. Håkansson, L. E. Fröberg, L. Samuelson, L. R. Wallenberg, *Nanotechnology* **2007**, *18*, 015504.
[15] E. Zintl, A. Harder, W. Haucke, *Z. Phys. Chem. Abt. B* **1937**, *35*, 354–362.
[16] C. Thelander, T. Mårtenson, M. T. Björk, B. J. Ohlsson, M. W. Larsson, L. R. Wallenberg, L. Samuelson, *Appl. Phys. Lett.* **2003**, *83*, 2052–2054.
[17] Y. N. Guo, J. Zou, M. Paladugu, H. Wang, Q. Gao, H. H. Tan, C. Jagadish, *Appl. Phys. Lett.* **2006**, *89*, 23 1917.
[18] K. A. Dick, K. Deppert, L. S. Karlsson, L. R. Wallenberg, S. Samuelson, W. Seifert, *Adv. Funct. Mater.* **2005**, *15*, 1603–1610.
[19] H. D. Park, S. M. Prokes, R. C. Cammarata, *Appl. Phys. Lett.* **2005**, *87*, 063110.
[20] K. A. Dick, Z. Geretovszky, A. Mikkelsen, L. S. Karlsson, E. Lundgren, J.-O. Malm, J. N. Andersen, L. Samuelson, W. Seifert, B. A. Wacaser, K. Deppert, *Nanotechnology* **2006**, *17*, 1344–1350.
[21] G. V. Raynor, in *Phase Diagrams of Ternary Gold Alloys* (Eds: A. Prince, G. V. Raynor, D. S. Evans), Institute of Metals, London 1990, pp. 294–300.
[22] C. T. Tsai, R. S. Williams, *J. Mater. Res.* **1986**, *1*, 352–360.
[23] S. Kodambaka, J. Tersoff, M. C. Reuter, F. M. Ross, *Science* **2007**, *4*, 729–732.
[24] N. E. Christensen, S. Satpathy, Z. Pawlowska, *Phys. Rev. B* **1987**, *36*, 1032–1050.
[25] M. Yazawa, M. Koguchi, K. Hiruma, *Appl. Phys. Lett.* **1991**, *58*, 1080–1082.
[26] Th. Schmidt, R. Kröger, T. Clausen, J. Falta, A. Janzen, M. Kammler, P. Kury, P. Zahl, M. Horn-von Hoegen, *Appl. Phys. Lett.* **2005**, *86*, 11 1910.
[27] K. Kawaguchi, M. Ekawa, T. Akiyama, H. Kuwatsuka, M. Sugawara, *J. Cryst. Growth* **2006**, *291*, 154–159.

Received: September 25, 2007
Revised: February 1, 2008

